A Model for a Shear-Free Convective Boundary Layer with Parameterized Capping Inversion Structure

E. E. FEDOROVICH*

Institut für Hydrologie und Wasserwirtschaft, Universität Karlsruhe, Karlsruhe, Germany

D. V. MIRONOV

Institute of Limnology, Russian Academy of Sciences, St. Petersburg, Russia

(Manuscript received 8 March 1994, in final form 17 May 1994)

ABSTRACT

The paper extends Deardorff's general structure parameterization for a shear-free convective boundary layer. The model suggested employs the mixed layer hypothesis that the buoyancy (which is defined as $b = g(\rho_0 - \rho)/\rho_0$, where ρ is the density, ρ_0 is the reference density, and g is the acceleration due to gravity) is constant with height within the mixed layer. The buoyancy flux zero-crossing height is taken as the mixed layer depth. The vertical buoyancy profile within the capping inversion, where the buoyancy flux is negative due to entrainment, is made dimensionless, using the buoyancy difference across the inversion and its thickness as appropriate scales. The approach was first suggested by Kitaigorodskii and Miropolsky for the oceanic seasonal thermocline. The authors examine the idea against the data from atmospheric measurements, laboratory experiments with buoyancy-agitated turbulence, and large-eddy simulations.

The rate equations for the mixed layer and inversion layer depths are derived using the turbulent kinetic energy equation and Deardorff's scaling hypothesis refined to account for the inversion layer structure. The constants of the model are evaluated from the data of atmospheric, oceanic, and laboratory measurements, and large-eddy simulations. The causes of divergence of the estimates based on data of different origin are discussed.

The model is applied to simulate convective entrainment in laboratory experiments. A reasonable explanation for ambiguous behavior of the entrainment zone in the experiments with a two-layer fluid is suggested. The model is found to simulate transition regimes of convective entrainment in multilayer fluid strongly affected by the nonstationarity of the entrainment zone.

1. Introduction

A convective boundary layer driven by temperature and moisture fluxes at the ground commonly develops during daytime over land surfaces. Deepening of the upper mixed layer in the ocean or in lakes due to surface cooling and/or its salinization is one more geophysical example of penetrative convection. In all these cases, growth of a convectively mixed layer occurs on a background of stable stratification. Between the well-mixed layer adjacent to the surface and the quiescent layer, there is an interfacial layer with strong stable density stratification (capping inversion in the atmosphere, thermocline/halocline in the ocean). In many instances the buoyancy production of turbulent kinetic energy in the convective boundary layer considerably dominates over its production due to velocity shear, so the layer can be taken as shear-free. The purpose of this paper is to develop a model for the shear-free convective boundary layer with the particular emphasis on evaluating the thickness of the interfacial layer and a realistic representation of the buoyancy structure within this layer.

Figure 1 shows the vertical profiles of buoyancy b and vertical turbulent buoyancy flux B in the initially linearly stratified fluid heated from below. The buoyancy is defined here as $b = g(\rho_0 - \rho)/\rho_0$, where ρ is the density, ρ_0 is the reference density, and g is the acceleration due to gravity. Resulting from heating, a well-mixed layer forms in the lower part of the fluid. This layer proves to be nearly homogeneous, so the buoyancy can be considered as height constant. In the near vicinity of the surface the buoyancy drops considerably with height from a surface value b_s to the mixed layer value b_m. The homogeneous mixed layer is separated from the nonturbulent layer aloft (which is linearly stratified with the vertical buoyancy gradient $db/dz = N^2$, where z is the height and N is the buoyancy

* On leave from the Main Geophysical Observatory, St. Petersburg, Russia.

Corresponding author address: Dr. E. Fedorovich, Institut für Hydrologie und Wasserwirtschaft, Universität Karlsruhe, Kaiserstraße 12, 76128 Karlsruhe, Germany.
E-mail: gg07@dkauni2.bitnet

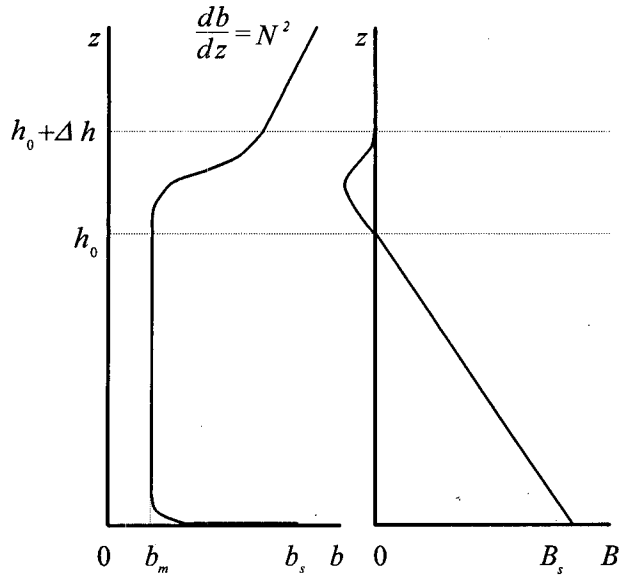

FIG. 1. Schematic pattern of the vertical profiles of buoyancy and turbulent buoyancy flux with nonsteady penetrative convection.

frequency) by an interfacial layer, where the buoyancy increases sharply with height. The kinetic energy of buoyant thermals is spent here for penetration of the mixed-layer turbulence into the more buoyant stably stratified fluid and for entrainment downward. The vertical turbulent buoyancy flux decreases linearly with height in the main part of the mixed layer. Its zero-crossing height roughly defines the mixed layer depth h_0. Being negative over the interfacial layer, B reaches a minimum at certain level within this level and vanishes toward its upper boundary $z = h_0 + \Delta h$. Thus, four regions can be distinguished in the fluid: the surface layer (whose depth is typically very small as compared to h_0), the mixed layer (ML), the interfacial layer (IL), and the nonturbulent layer.

The convective boundary layer has been extensively studied using the zero order jump model (Lilly 1968). Vertical profiles of mean buoyancy and vertical buoyancy flux for this model are shown in Fig. 2. The capping inversion is represented by the zero order buoyancy jump $\Delta b'$ at a level $z = \bar{h}$ within the interfacial layer and the negative buoyancy flux of entrainment $B_h = -\Delta b' d\bar{h}/dt$, where t is the time. As can be seen from the plot, the zero order buoyancy increment $\Delta b'$ is not equal to the actual buoyancy difference Δb across the IL, and B_h is not equal to the most negative flux of entrainment. The zero order approach has been successfully applied to predict the entrainment rate $d\bar{h}/dt$ as related to $\bar{h}$, $\Delta b'$, N, and the surface buoyancy flux B_s. If the quantities $\Delta b'$, N, and B_s are known, any reasonable assumption on B_h closes the problem. Ball (1960) suggested that $-B_h = B_s$, which corresponds to the maximum possible entrainment rate. The case of minimum entrainment, when $\Delta b' = 0$ and the entrainment equation has the form $d\bar{h}/dt = B_s/(N^2\bar{h})$, was first discussed by Zubov (1945). This regime is referred to as "encroachment" (see Carson and Smith 1974). The intermediate cases, $0 < -B_h/B_s < 1$, were considered by Betts (1973), Carson (1973), Tennekes (1973), Stull (1973), Zilitinkevich (1975), and Zeman and Tennekes (1977), among others. The most comprehensive zero order jump model comprising the aforementioned ones as the asymptotic cases was suggested by Zilitinkevich (1991).

Based upon the experimental evidence that the buoyancy increment Δb occurs over a layer of significant thickness, Betts (1974) proposed the first-order jump model. The model assumes that the mixed layer extends up to the height of the most negative buoyancy flux of entrainment, and that b and B increase linearly with height within the interfacial layer, undergoing the first-order discontinuities at its upper and lower boundaries (Fig. 3). The drawbacks of the model are that the profiles of b and B in the interfacial layer are hardly the linear ones in reality, and that the minimum buoyancy flux of entrainment occurs within the IL, not at its bottom. Thus, the IL thickness in the first-order jump model, $\Delta h'$, is significantly smaller than the actual one (Δh in Fig. 1).

The next step toward parameterization of the convective boundary layer was made by Deardorff (1979), who allowed all the negative buoyancy flux of entrainment to take place within the IL. The structure of the

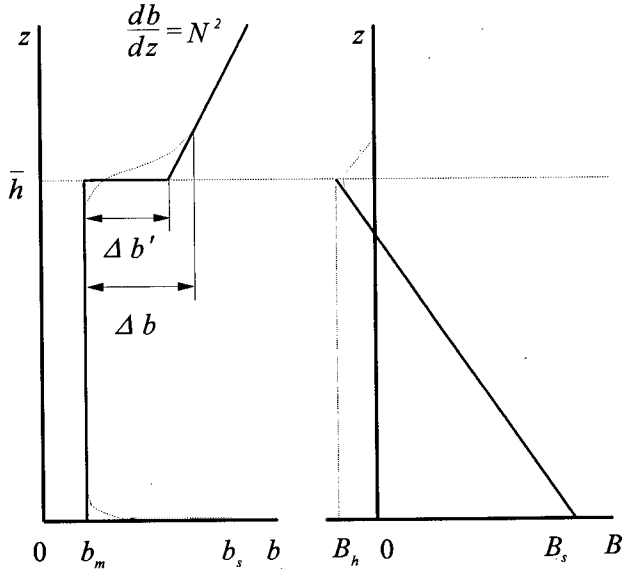

FIG. 2. Vertical profiles of buoyancy and buoyancy flux for the zero order jump model. The dashed lines indicate actual profiles, and the solid lines correspond to parameterization, where $\Delta b'$ is the difference between the value of buoyancy obtained by the linear extrapolation from the nonturbulent layer down to the level $z = \bar{h}$ and the mean buoyancy in the mixed layer.

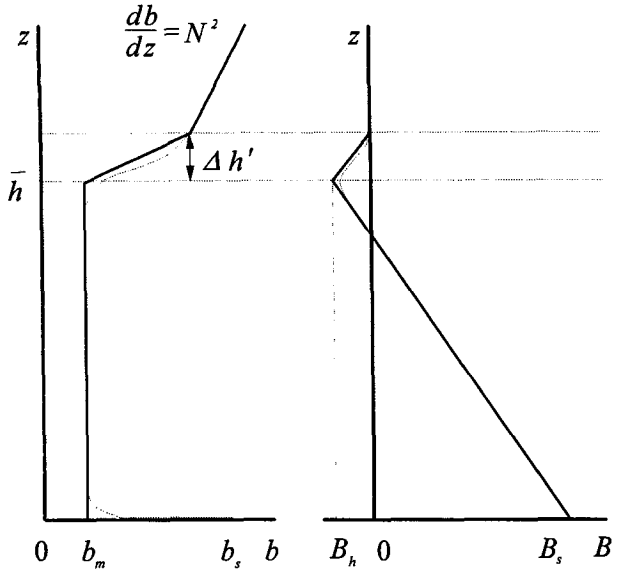

FIG. 3. Vertical profiles of b and B for the first-order jump model. The dashed lines show actual profiles, and the solid lines correspond to the parameterization, where $\Delta h'$ is the IL thickness.

IL is described in Deardorff's model in a more realistic way. The buoyancy profile is represented in the form

$$b = b_m + F\Delta b, \tag{1}$$

where F is a dimensionless function of height. After the integration of the buoyancy transfer equation [Eq. (5) in the next section] over the IL depth an integral shape factor

$$C_b = \Delta h^{-1} \int_{h_0}^{h_0+\Delta h} F dz \tag{2}$$

appears in the expression for the IL buoyancy budget. The shape factor is assumed to depend on relative stratification $G = N^2(\Delta h/\Delta b)$, that is, on the square of the ratio of N and mean buoyancy frequency in the IL, $(\Delta b/\Delta h)^{1/2}$. The empirical approximation of $C_b(G)$ was suggested in Deardorff; however, the form of the function F was not determined.

The model performed well in the cases of steady-state entrainment with large-scale subsidence ($dh_0/dt = d\Delta h/dt = d\Delta b/dt = 0$) and pseudoencroachment ($d\Delta h/dt = d\Delta b/dt = 0$ and $G = 1$), when no closure assumption on dh_0/dt or $d\Delta h/dt$ is required. For unsteady entrainment a quite arbitrary closure assumption was made on $d\Delta/dt$, which seems to be a fitting relation rather than the theoretically substantiated entrainment equation. Furthermore, it does not provide for free entrainment at $N = 0$ (it leads to ambiguous expression for $d\Delta h/dt$ as Δb and Δh become small).

In the present paper a model for a shear-free convective boundary layer is developed. A three-layer parameterization is used for the vertical buoyancy profile, including a buoyancy homogeneous well-mixed layer, an interfacial entrainment layer, and a neutrally or stably stratified nonturbulent layer aloft. The entrainment rate equation is derived on the basis of equation for turbulent kinetic energy using the hypothesis of similarity for convective boundary layers (Deardorff 1970a,b) revised to account for the interfacial layer structure. An attempt is also made to find a reasonable approximation for buoyancy profile within the IL, using the concept of Kitaigorodskii and Miropolsky (1970).

Kitaigorodskii and Miropolsky introduced the temperature difference across the oceanic seasonal thermocline, ΔT, and its thickness, Δh, as the appropriate temperature and depth scales. They found that a number of temperature profiles obtained at ocean weather ships are fairly well represented by the universal dependence of dimensionless temperature $[T(z) - T_m]/\Delta T$, where T_m is the mixed-layer temperature on dimensionless depth $(z - h_0)/\Delta h$. The concept was then used to process the data from laboratory experiments (Linden 1975; Wyatt 1978). However, it has never been applied to the inversion capping the atmospheric boundary layer.

Now we give an outline of the paper. In section 2 the representation of the vertical buoyancy profile and the buoyancy budget equations are considered. The entrainment rate equation is derived in section 3. The model parameters are evaluated in section 4, using atmospheric, oceanic, and laboratory data, and results of large-eddy simulations. In section 5 the results of numerical experiments are discussed and compared with laboratory data.

2. Parameterization of the vertical buoyancy profile and the buoyancy budget

We simplify the discussion by considering a horizontally homogeneous boundary layer without large-scale subsidence. Let us assume that with the development of convection the vertical buoyancy profile keeps the following form:

$$b = \begin{cases} b_m & \text{at } 0 \leqslant z \leqslant h_0 \\ b_m + \Delta b F(\zeta, G) & \\ \qquad \text{at } h_0 \leqslant z \leqslant h_0 + \Delta h & \\ b_m + \Delta b + N^2(z - h_0 - \Delta h) & \\ \qquad \text{at } h_0 + \Delta h \leqslant z. & \end{cases} \tag{3}$$

The quiescence of the nonturbulent layer, adopted in the model, implies that within this layer some initial linear buoyancy profile $b_0(z)$ is conserved, and $b(z, t) = b_0(z)$ at $z \geqslant h_0 + \Delta h$.

In the representation (3), F is the function of dimensionless coordinate $\zeta = (z - h_0)/\Delta h$ and stratification parameter G, satisfying conditions

$$F|_{\zeta=0} = \left.\frac{\partial F}{\partial \zeta}\right|_{\zeta=0} = 0, \quad F|_{\zeta=1} = 1, \quad \left.\frac{\partial F}{\partial \zeta}\right|_{\zeta=1} = G. \quad (4)$$

The parameterization (3) omits the difference between b_m and the buoyancy in the thin surface layer (Fig. 1). Its little contribution to the total buoyancy budget can be neglected.

The evolution of the buoyancy profile (3) should satisfy the buoyancy transfer equation

$$\frac{\partial b}{\partial t} = -\frac{\partial B}{\partial z}. \quad (5)$$

Molecular transfer plays an insignificant part in the atmosphere and in the ocean; hence, it is neglected in Eq. (5).

Integrating Eq. (5) over z from 0 to h_0 with due regard to the representation (3) and taking into account the definition of the mixed layer depth as the buoyancy flux crossover height, $B = 0$ at $z = h_0$, we obtain the mixed layer buoyancy budget equation (see appendix for details of derivation):

$$\frac{d}{dt}[N^2(h_0 + \Delta h) - \Delta b] = \frac{B_s}{h_0}. \quad (6)$$

Integration of Eq. (5) over z from 0 to $h_0 + \Delta h$ gives the equation of total buoyancy budget:

$$\frac{d}{dt}\left\{\frac{1}{2}N^2(h_0 + \Delta h)^2 - \Delta b[h_0 + (1 - C_b)\Delta h]\right\} = B_s, \quad (7)$$

where $C_b(G) = \int_0^1 F(\zeta, G)d\zeta$ is the integral shape factor.

In accordance with (3) and (5), the vertical turbulent buoyancy flux decreases linearly with height within the mixed layer, at $0 \leq z \leq h_0$:

$$B = B_s(1 - z/h_0). \quad (8)$$

In the interfacial layer, at $h_0 \leq z \leq h_0 + \Delta h$, its profile has the form

$$B = \left[\int_0^\zeta F(\zeta', G)d\zeta' - G\frac{\partial}{\partial G}\int_0^\zeta F(\zeta', G)d\zeta' - \zeta\right]\frac{\Delta h}{h_0}B_s + \left[F - G\int_0^\zeta F(\zeta', G)d\zeta' + G^2\frac{\partial}{\partial G}\int_0^\zeta F(\zeta', G)d\zeta'\right]\Delta b\frac{dh_0}{dt} + \left[\zeta F - (1 + G)\int_0^\zeta F(\zeta', G)d\zeta' - G(1 - G)\frac{\partial}{\partial G}\int_0^\zeta F(\zeta', G)d\zeta'\right]\Delta b\frac{d\Delta h}{dt}. \quad (9)$$

Equations (6) and (7) are the two ordinary differential equations for three unknowns: h_0, Δh, and Δb. An additional relation is needed to close the problem, namely, the entrainment rate equation.

3. The entrainment rate equation

We employ the balance equation for turbulent kinetic energy (TKE):

$$\partial e/\partial t = B - \partial\Phi/\partial z - \epsilon, \quad (10)$$

where e is the turbulent energy per unit of fluid mass, ϵ is its viscous dissipation rate, and Φ is the vertical transport of energy.

We adopt the hypothesis of similarity of convective regime considered, which states that the basic turbulence parameters, being normalized by the length scale $h_0 + \Delta h$ and the velocity scale $w_* = [B_s(h_0 + \Delta h)]^{1/3}$, cease to depend on time in their explicit form and depend on it only through these scales; that is, they become universal functions of the dimensionless height $z/(h_0 + \Delta h)$. Hence, the vertical profiles of turbulent energy and its dissipation rate can be presented in the form

$$e = w_*^2 F_e\left(\frac{z}{h_0 + \Delta h}\right), \quad \epsilon = \frac{w_*^3}{h_0 + \Delta h}F_\epsilon\left(\frac{z}{h_0 + \Delta h}\right), \quad (11)$$

where F_e and F_ϵ are the dimensionless functions satisfying boundary conditions $F_e(1) = F_\epsilon(1) = 0$.

The employed closure hypothesis is very similar to the one proposed by Deardorff (1970a,b), which has been widely used in zero order jump models. Instead of the quite arbitrary height $\bar{h}$ within the limits of the IL (usually close to the height of the buoyancy flux minimum), we use $h_0 + \Delta h$, that is, the depth of the whole turbulized zone, as an appropriate length scale. This allows one to reduce the scatter of points in the interfacial layer in Figs. 4 and 6, showing the data on turbulent energy and its dissipation rate from the field and laboratory measurements. The height $\bar{h}$ is suitable for scaling the turbulence parameters in the major part of the convective boundary layer, but not within the IL (Zilitinkevich 1991). Utilization of $h_0 + \Delta h$ decreases the range of empirical estimates of the universal functions for ϵ and e precisely near the boundary layer top.

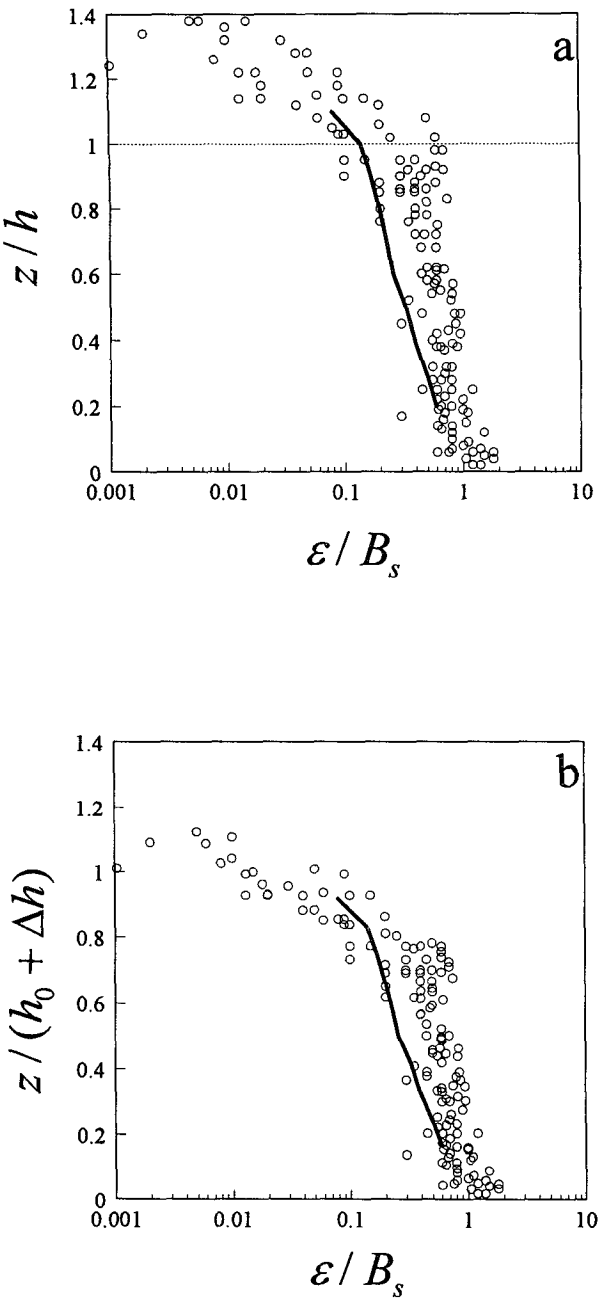

FIG. 4. Empirical dependencies of dimensionless dissipation rate of turbulent kinetic energy, ϵ/B_s, on dimensionless height: (a) $z/\bar{h}$ and (b) $z/(h_0 + \Delta h)$. The points are the data from measurements in the atmospheric boundary layer (Caughey and Palmer 1979; Lenschow et al. 1980) and in the ocean (Shay and Gregg 1986). The line is from the Deardorff and Willis (1985) laboratory experiments. When the profiles of turbulent buoyancy flux were not given, the depth of the boundary layer, $h_0 + \Delta h$, was determined as the crossover height of the best-fit curve.

The distinctions between the TKE and dissipation rate profiles from large-eddy simulations (LES) of convection by different authors, originating primarily from the differences in the employed parameterizations for the subgrid turbulence, were analyzed by Nieuwstadt et al. (1993). As seen from the normalized profiles in

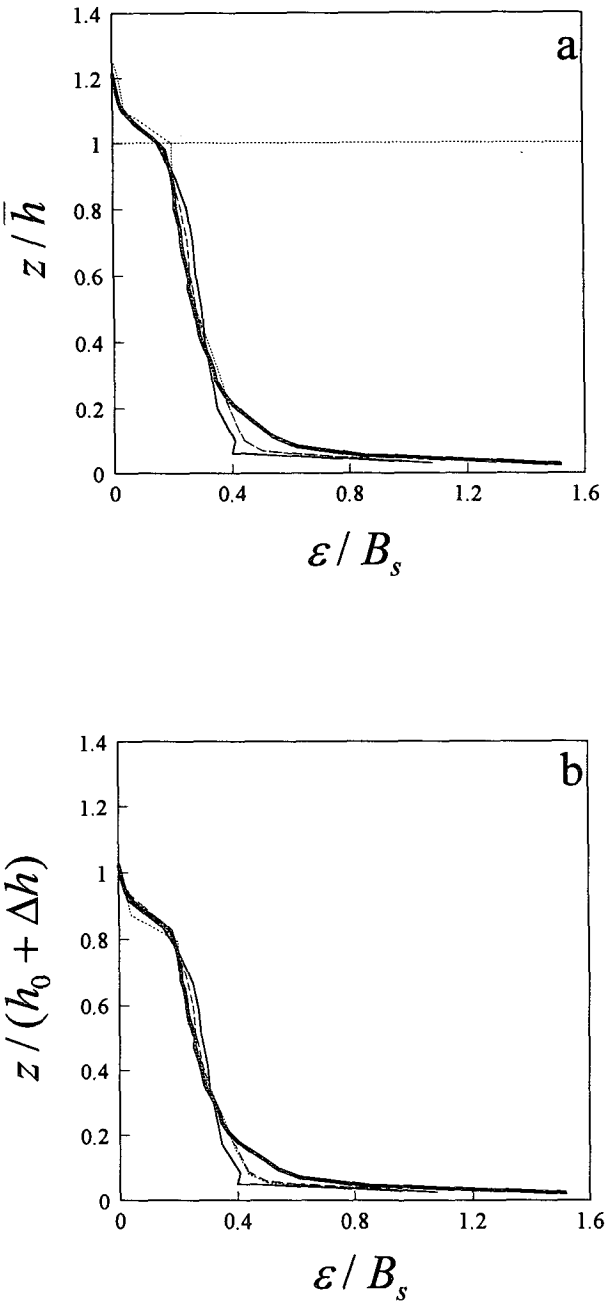

FIG. 5. Distribution of turbulence dissipation rate in the atmospheric convective boundary layer from LES (Nieuwstadt et al. 1993): (a) z is scaled by $\bar{h}$, and (b) z is scaled by $h_0 + \Delta h$. The heavy solid line shows Mason's (1989) results, and the solid line is from Moeng's (1984) simulations; calculations by Nieuwstadt and Brost (1986) and Schmidt and Schumann (1989) are shown by dotted and dashed lines, respectively.

Figs. 5 and 7, the scaling based on $h_0 + \Delta h$ does not induce, to say the least, any additional discrepancies in the data of LES.

Using (8), (9), and (11), the termwise integration of Eq. (10) over z from 0 to $h_0 + \Delta h$ gives the following entrainment rate equation:

$$\frac{10}{3} C_e \left(1 + \frac{\Delta h}{h_0}\right)^{2/3} (E_h + E_\Delta) = (1 - 2C_\epsilon) - 2C_\epsilon \frac{\Delta h}{h_0} - \left(1 - 2C_{bb} + 2G\frac{dC_{bb}}{dG}\right)\left(\frac{\Delta h}{h_0}\right)^2 + 2\left(C_b - GC_{bb} + G^2\frac{dC_{bb}}{dG}\right)\frac{\Delta h}{h_0}\mathrm{Ri}_b E_h + 2\left[C_b - 2C_{bb} - GC_{bb} - G(1-G)\frac{dC_{bb}}{dG}\right]\frac{\Delta h}{h_0}\mathrm{Ri}_b E_\Delta - \frac{4}{3} C_e \left(1 + \frac{\Delta h}{h_0}\right)^{5/3} De - 2\frac{\Phi(h_0 + \Delta h)}{B_s h_0}, \quad (12)$$

where $E_h = (B_s h_0)^{-1/3} dh_0/dt$ is the dimensionless entrainment rate; $E_\Delta = (B_s h_0)^{-1/3} d\Delta h/dt$ is the dimensionless rate of changes of Δh; $\mathrm{Ri}_b = B_s^{-2/3} h_0^{1/3} \Delta b$ is the Richardson number based on the buoyancy increment across the IL; $De = B_s^{-4/3} h_0^{2/3} dB_s/dt$ is the nonstationarity parameter introduced in Deardorff et al. (1980) [following Zilitinkevich (1991) we call it the Deardorff number]; $C_e = \int_0^1 F_e(x)dx$ and $C_\epsilon = \int_0^1 F_\epsilon(x)dx$ are dimensionless constants; $C_{bb} = \int_0^1 d\zeta \int_0^\zeta F(\zeta', G)\zeta'$ is a dimensionless function of G; and $\Phi(h_0 + \Delta h)$ is the energy flux at the boundary layer top.

The energy escape from the boundary layer occurs due to the radiation of internal gravity waves into the stably stratified layer aloft. The maximum flux of energy expended for maintenance of propagating waves is expressed by (Thorpe 1973)

$$\Phi_{\max} = (3\pi\sqrt{3})^{-1} N^3 A^2 \lambda, \quad (13)$$

where A and λ are the amplitude and length of the waves, respectively. In the framework of the simple bulk approach A and λ are usually determined from the similarity arguments.

Kantha (1977) assumed the wave amplitude to be of the order of the IL thickness, while the wavelength is proportional to the mixed-layer depth h_0. This yields

$$2\frac{\Phi(h_0 + \Delta h)}{B_s h_0} = C_N \mathrm{Ri}_N^{3/2} \left(\frac{\Delta h}{h_0}\right)^2, \quad (14a)$$

where $\mathrm{Ri}_N = B_s^{-2/3} h_0^{4/3} N^2$ is the Richardson number based on the buoyancy frequency in the nonturbulent layer, and C_N is a dimensionless constant.

Zilitinkevich (1991) argued that both A and λ are of the order of Δh, which gives

$$2\frac{\Phi(h_0 + \Delta h)}{B_s h_0} = C'_N \mathrm{Ri}_N^{3/2} \left(\frac{\Delta h}{h_0}\right)^3, \quad (14b)$$

where C'_N is another dimensionless constant. There is no consensus on which expression of (14a) and (14b) is adequate. In section 5 we will attempt to verify both against the data from laboratory experiments.

Thus, Eqs. (6), (7), (12), and (14a) or (14b) constitute a closed set. The dimensionless constants C_ϵ, C_e, and C_N or C'_N and the shape factors $C_b(G)$ and $C_{bb}(G)$ should be determined from empirical data.

4. The model constants and empirical relations

The constants C_ϵ and C_e are evaluated by integrating the functions F_ϵ and F_e in Eq. (11), obtained from measurements and large-eddy simulations of convection, over the whole turbulized zone. The estimates are given in Table 1.

For C_ϵ the atmospheric and oceanic data give similar values, which, however, considerably exceed the laboratory and LES ones. This discrepancy is probably due to the contribution of velocity shear into the total energy budget, which was neither present in laboratory conditions nor taken into account in the large-eddy simulations we consider herein. The laboratory and LES estimates are close to each other.

For C_e the atmospheric estimates diverge considerably. Integration of function F_e obtained with LES gives smaller values of this constant compared to those derived from both atmospheric and laboratory data. Considerable difference between laboratory and LES estimates may be explained by the contribution of horizontal velocity fluctuations in the laboratory tank, induced by the large-scale bottom temperature variations in the horizontal (see discussion in Schmidt and Schumann 1989). We adopt the values $C_\epsilon = 0.3$ and $C_e = 0.3$ as most appropriate for the shear-free case.

We know of no direct measurements of the vertical energy flux at the IL top. Therefore, the dimensionless constants in Eqs. (14a) and (14b) should be estimated by comparing theoretical and empirical entrainment laws, that is, the dependencies of the entrainment rate upon the Richardson numbers specified above. This can also be a way to decide between the two expressions for wave-related vertical energy flux.

Now we have to determine the function $F(\zeta, G)$. Kitaigorodskii and Miropolsky (1970) approximated the dimensionless temperature profile in oceanic seasonal thermocline by the fourth-order polynomial of ζ.

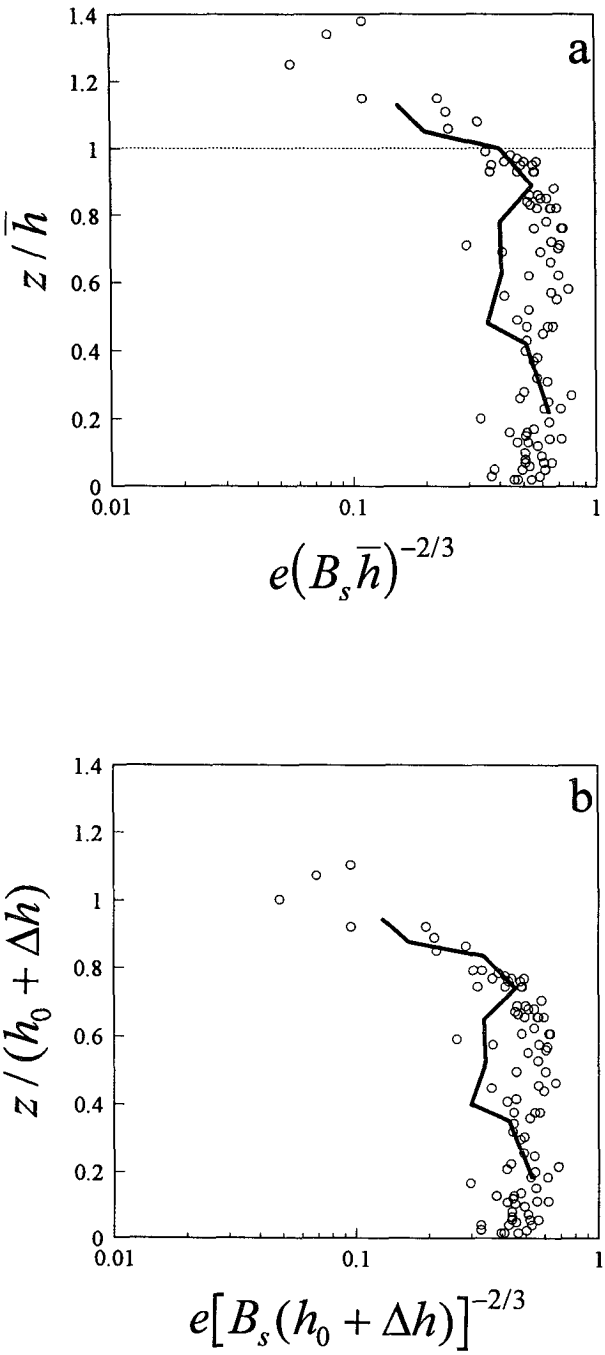

FIG. 6. Empirical vertical profiles of turbulent kinetic energy. (a) The energy is scaled by $(B_s\bar{h})^{2/3}$, and the height is scaled by $\bar{h}$; (b) the scales are $[B_s(h_0 + \Delta h)]^{2/3}$ and $h_0 + \Delta h$, respectively. The points are the atmospheric data of Caughey and Palmer (1979) and Lenschow et al. (1980), respectively; the line represents the laboratory measurements of Deardorff and Willis (1985).

Similar expressions were suggested by Linden (1975) and Wyatt (1978) using data from laboratory experiments, and by Miropolsky et al. (1970), Reshetova and Chalikov (1977), Efimov and Tsarenko (1980), and Malkki and Tamsalu (1985) on the basis of field measurements. However, the empirical points revealed a wide scatter about the curves $F(\zeta)$.

The theoretical background for the Kitaigorodskii and Miropolsky concept was provided by Barenblatt (1978), Turner (1978), Shapiro (1980), and Zilitinkevich and Mironov (1992). In the case of mixed layer deepening with a constant entrainment rate and con-

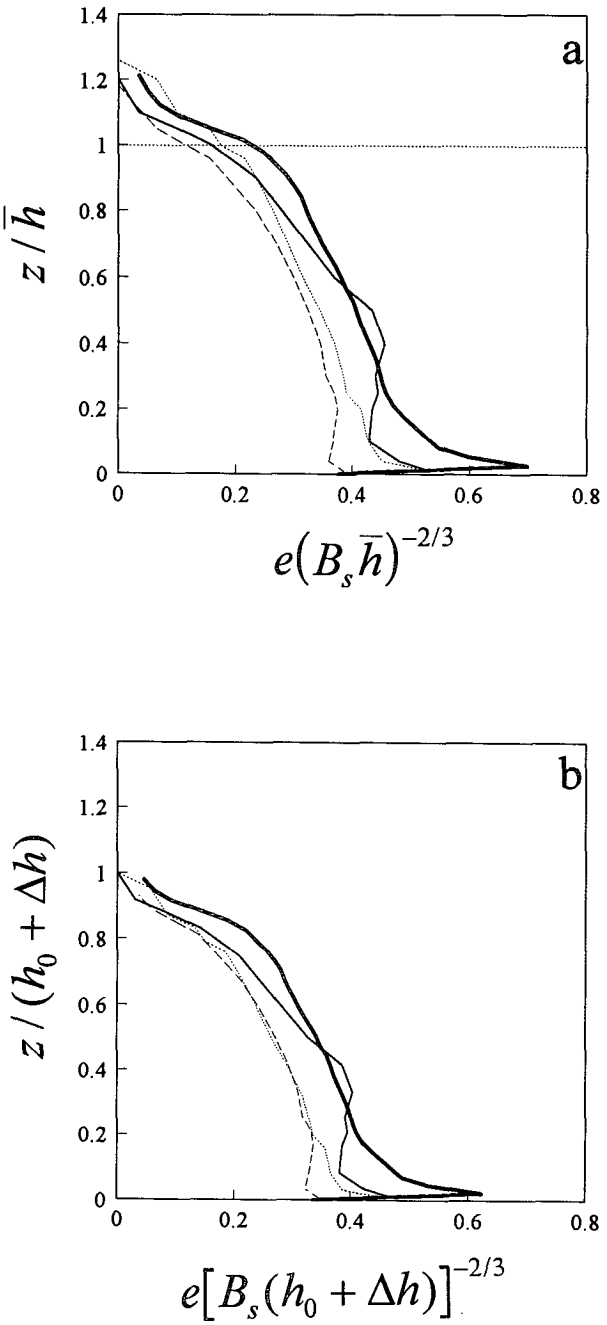

FIG. 7. Turbulent kinetic energy as a function of dimensionless height from LES. See Fig. 5 for details.

TABLE 1. Estimates of dimensionless constants C_ϵ and C_e in the entrainment rate equation, obtained by integration of the functions F_ϵ and F_e.

Reference	C_ϵ	C_e
Measurements in the atmosphere		
Caughey and Palmer (1979)	0.53	0.46
Lenschow et al. (1980)	0.48	0.31
Average from atmospheric measurements	**0.51**	**0.38**
Measurements in the ocean		
Shay and Gregg (1986)	0.58	—
Laboratory experiments		
Deardorff and Willis (1985)	0.34	0.42
Large-eddy simulations		
Mason (1989)	0.30	0.32
Moeng (1984)	0.29	0.29
Nieuwstadt and Brost (1986)	0.28	0.25
Schmidt and Schumann (1989)	0.29	0.24
Average from large-eddy simulations	**0.29**	**0.28**

stant temperatures at the IL boundaries, temperature profile was found to be self-similar, given by the propagating wave–type solution of the heat transfer equation

$$\frac{\partial T}{\partial t} = \frac{\partial}{\partial z} K_H \frac{\partial T}{\partial z},$$

where K_H is the heat conductivity. In the case of a collapsing mixed layer, no theoretical explanation of the thermocline self-similarity has been suggested so far.

The convective boundary layer corresponds to the case of a mixed layer deepening. In fact neither entrainment rate nor the temperatures at the IL boundaries are constant in time. Yet one can expect the approximate self-similarity of the buoyancy profile in the IL, if these quantities vary slowly with time (Zilitinkevich and Mironov 1992).

An approximation of the function $F(\zeta, G)$ that fits atmospheric and laboratory data reasonably well can be obtained from geometrical arguments. To match the continuity conditions (4) we may represent the required function in the form of a fourth-order polynomial whose coefficients should be the functions of C_b to satisfy the additional integral condition (2). This gives the following approximation for the dimensionless buoyancy profile:

$$F(\zeta, G) = \left(\frac{3}{2}G - 12 + 30C_b\right)\zeta^2 + (28 - 4G - 60C_b)\zeta^3 + \left(\frac{5}{2}G - 15 + 30C_b\right)\zeta^4, \quad (15)$$

where the dependence of the integral shape factor C_b on the relative stratification G is to be found empirically.

Figure 8 shows the dependence of C_b on G. The majority of C_b values lie between 0.35 and 0.55. The maximum value corresponding to the two-layer fluid system is 0.57. Within the observed range of G variations exponential function proposed by Deardorff (1979),

$$C_b = 0.55 \exp(-0.27G) \quad (16)$$

fits the empirical data fairly well.

According to (15), function $C_{bb}(G)$ in Eq. (12) is

$$C_{bb} = \frac{1}{120}G - \frac{1}{10} + \frac{1}{2}C_b. \quad (17)$$

The empirical dependence of C_{bb} on G is shown in Fig. 9 together with the curve calculated from Eqs. (16) and (17). The scatter of points about the curves in Figs. 8 and 9 is rather small despite the different sources of the data. This justifies the use of a simple polynomial profile (15), at least as a first approximation.

5. Comparison with laboratory data

The model described in the previous sections assumes that mean velocity shear has only a minor contribution to the total energy budget. Very few atmospheric data match this assumption. Shear-free penetrative convection was thoroughly studied in the series of laboratory experiments by Deardorff et al. (1969,

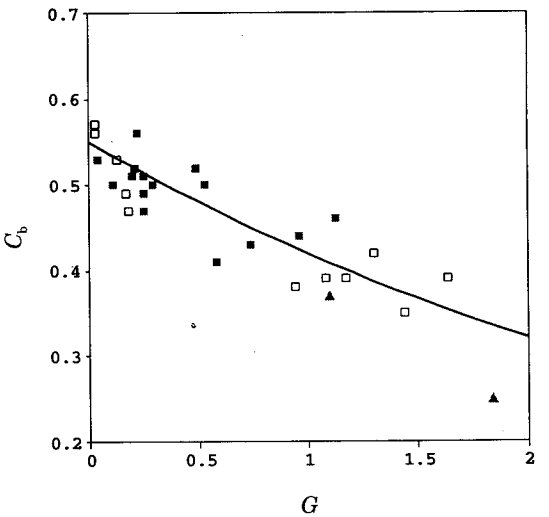

FIG. 8. The integral shape factor C_b as function of relative stratification G. The open squares are laboratory data (Deardorff 1979; Deardorff et al. 1980; Deardorff and Willis 1985); the filled squares represent atmospheric data of Clarke et al. (1971), Chorley et al. (1975), Batchvarova and Gryning (1991), and Gryning and Batchvarova (1994); and the triangles depict LES results of Mason (1989) and Schmidt and Schumann (1989). The line shows approximation (16).

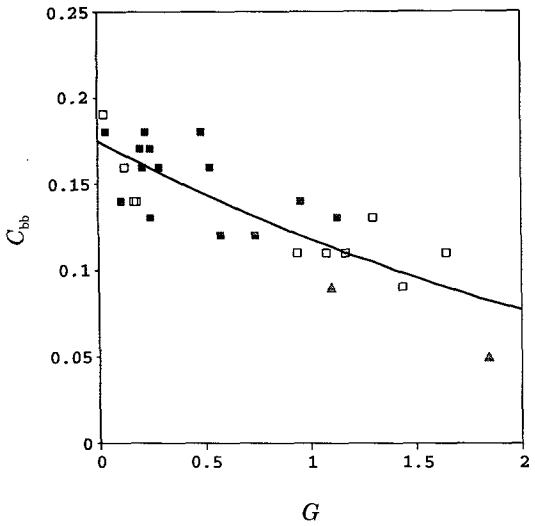

FIG. 9. The dependence of dimensionless parameter C_{bb} on relative stratification G. Markers are the same as in Fig. 8. The curve is drawn after Eqs. (16) and (17).

1980; Willis and Deardorff 1974; Deardorff and Willis 1985). The most comprehensive dataset was presented in Deardorff et al. (1980, hereafter DWS). It will be used to test our model.

The results of laboratory experiments and model simulations are conveniently represented in the form of an entrainment law. A traditional way originating from the zero order jump approach is to express the entrainment rate and Richardson numbers in terms of $\bar{h}$, as follows:

$$\bar{E} = (B_s\bar{h})^{-1/3}d\bar{h}/dt, \quad \overline{\mathrm{Ri}_b} = B_s^{-2/3}\bar{h}^{1/3}\Delta b,$$

$$\overline{\mathrm{Ri}_N} = \frac{1}{2}B_s^{-2/3}\bar{h}^{4/3}N^2. \quad (18)$$

Our model allows us to determine $\bar{h}$ directly from the shape of the buoyancy flux profile (9) as the height of B minimum within the entrainment zone. In the model runs, the variations of the bottom buoyancy flux with time were neglected in the entrainment equation, as they are not important in most interesting cases, including the DWS experiments (see Zilitinkevich 1991). While solving numerically the model system, all variables in Eqs. (6), (7), and (12) were normalized using B_s and the initial value of the ML depth as scales. The results of the model calculations, presented below, are obtained with the initial value of normalized $h_0 = 1$.

The entrainment relation for a two-layer fluid ($\overline{\mathrm{Ri}_N} = 0$), calculated by the model with initial values of $\Delta h = 0$ and $\mathrm{Ri}_b = 100$, is depicted in Fig. 10. We use here the traditional terminology, speaking about a "two-layer fluid," though in reality it is a three-layer one: mixed layer, interfacial layer, and nonturbulent neutral layer. Within the zero order approach this is really a two-layer fluid because the interfacial layer is reduced to the zero-thickness surface. The initial conditions for normalized h_0 and Δb define the initial Richardson number Ri_b. Depending upon the initial Δh value, dimensionless entrainment rate does not reveal unique dependence on Richardson number at the early stage of the buoyancy profile evolution when nonstationarity of the entrainment zone plays an important part. However, as time passes, the curves corresponding to different initial $\Delta h/h_0$ converge to a unique one showing a quasi-equilibrium entrainment regime. The initial period of adjustment is not illustrated in the plot.

The model predictions agree well with the data from two-layer fluid experiments of DWS. The dependence of $\bar{E}$ versus $\overline{\mathrm{Ri}_b}$, shown in Fig. 10, practically coincides with the basic relation of the zero order model, $\bar{E}\cdot\overline{\mathrm{Ri}_b} = \mathrm{const}$.

If the nonturbulent layer is stably stratified, entrainment law relates $\bar{E}$ to the two Richardson numbers, $\overline{\mathrm{Ri}_b}$ and $\overline{\mathrm{Ri}_N}$. In Fig. 11 the product $\bar{E}\cdot\overline{\mathrm{Ri}_b}$ is plotted against $\overline{\mathrm{Ri}_N}$ (its initial value was set equal to 4 in the calculations presented, at initial $\overline{\mathrm{Ri}_b} = 1$), using two different parameterizations for wave-related energy flux at the boundary layer top. Dimensionless constants C_N and C'_N were estimated as the best fit to empirical data from the DWS experiments with the linearly stratified fluid.

At $\overline{\mathrm{Ri}_N} \gg 1$, which corresponds to strong static stability in the quiescent layer, Eq. (14a) results in the asymptotic entrainment relation $\bar{E} \propto \overline{\mathrm{Ri}_b}^{-1}\overline{\mathrm{Ri}_N}^{-3/4}$, while Eq. (14b) leads to $\bar{E} \propto \overline{\mathrm{Ri}_b}^{-1}\overline{\mathrm{Ri}_N}^{-1/2}$. Both entrainment relations were reported in literature (Fernando 1991). The overall difference between the two

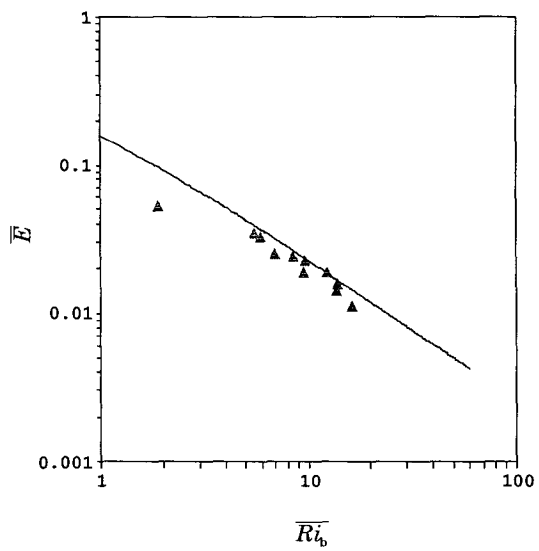

FIG. 10. Dimensionless entrainment rate $\bar{E}$ versus Richardson number $\overline{\mathrm{Ri}_b}$ for a two-layer fluid system. The model curve is shown by the solid line; the points are from the Deardorff et al. (1980) laboratory experiments.

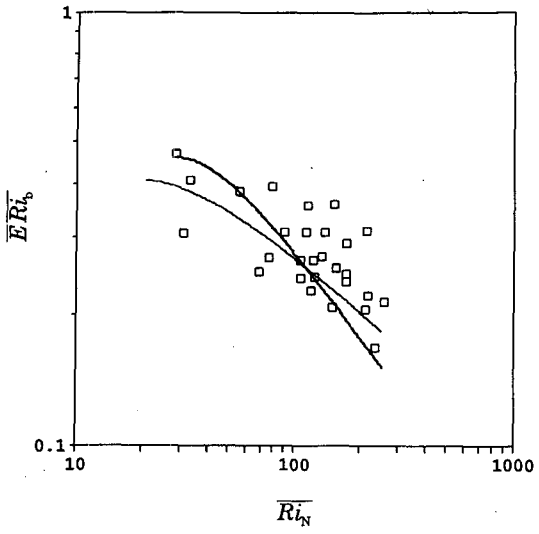

FIG. 11. The product $\bar{E} \cdot \overline{\mathrm{Ri}_b}$ versus Richardson number $\overline{\mathrm{Ri}_N}$ based on the buoyancy frequency in the nonturbulent layer. The heavy solid curve is calculated using Eq. (14a) with $C_N = 0.001$, and the solid line shows the results of calculation with Eq. (14b) and $C_N' = 0.012$; the points are from the Deardorff et al. (1980) laboratory experiments with a linearly stratified fluid.

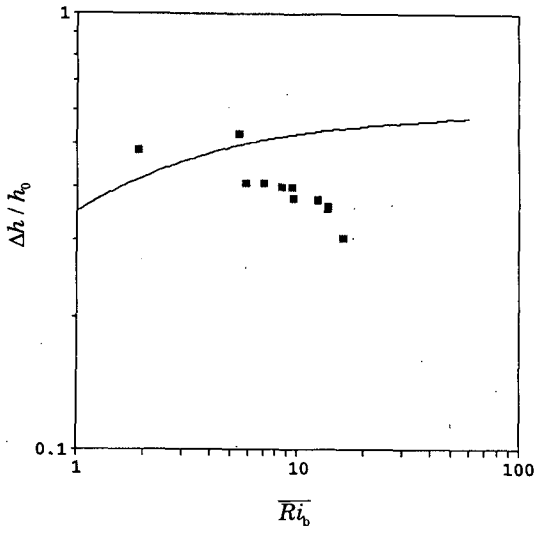

FIG. 12. Normalized entrainment layer depth $\Delta h/h_0$ versus $\overline{\mathrm{Ri}_b}$ in a two-layer fluid. The curve is calculated by the present model; the points are from the Deardorff et al. (1980) laboratory experiments.

parameterizations in Fig. 11 is rather small considering the data scatter. Still, the DWS data give more evidence to the $-1/2$ asymptote than to the $-3/4$ one.

The other important characteristic of entrainment is the ratio of the IL depth to that of the ML. Within the framework of the zero order jump approach $\Delta h/h_0$ is related to $\bar{E} \cdot \overline{\mathrm{Ri}_b}$ by the so-called geometric formula (Stull 1976; Zilitinkevich 1991), $\Delta h/h_0 = 2\bar{E} \cdot \overline{\mathrm{Ri}_b}$. The present model explicitly accounts for the nonstationarity of the entrainment zone, and, in some cases, dependence of $\Delta h/h_0$ on one or another stability parameter may be very different from that of $\bar{E} \cdot \overline{\mathrm{Ri}_b}$.

Figure 12 displays $\Delta h/h_0$ as function of $\overline{\mathrm{Ri}_b}$ in the two-layer fluid system. The prescribed initial values of these two parameters in the model run are the same as in Fig. 10. As seen from the plot, the model predicts $\Delta h/h_0$ to increase with increasing $\overline{\mathrm{Ri}_b}$, while the DWS data show weak inverse dependence. This fact cannot be explained by the zero order model that predicts $\Delta h/h_0$ to increase linearly at small $\overline{\mathrm{Ri}_b}$, approaching constant at $\overline{\mathrm{Ri}_b} \gg 1$. Our model allows reasonable explanation of the $\Delta h/h_0$ behavior in the DWS experiments.

Deardorff et al. (1980, p. 54) write, "In our experiments intended to treat a two-layer system, Δh usually decreased with time at first as the uppermost penetration height h_2 worked its way up toward the base of the preestablished neutral layer aloft. Then Γ was large. After h_2 reached this height, $\Delta h/h_0$ increased with time as $\Delta\theta$ and Ri_* decreased and Γ was small." In the present notation h_2 is $h_0 + \Delta h$, and Γ, $\Delta\theta$, and Ri_* correspond to N^2, Δb, and $\overline{\mathrm{Ri}_b}$, respectively.

All the foregoing means that entrainment occurs first in a linearly stratified fluid where $\Delta h/h_0$ decreases monotonically with $\overline{\mathrm{Ri}_b}$ (see Fig. 13). After the IL top has reached the base of the neutral layer, the entrainment zone evolves to achieve a quasi-equilibrium state characteristic of a two-layer fluid, passing the transition stage described above. At this stage of entrainment $\Delta h/h_0$ might reveal inverse dependence on $\overline{\mathrm{Ri}_b}$, caused by

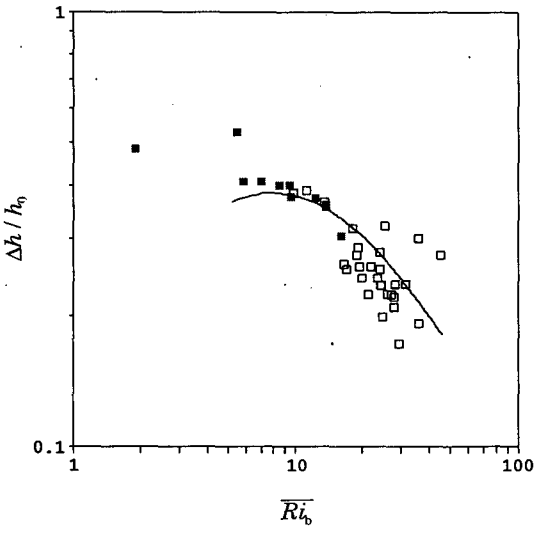

FIG. 13. Normalized entrainment layer depth $\Delta h/h_0$ versus $\overline{\mathrm{Ri}_b}$ in a linearly stratified fluid. The curve is calculated by the present model's (6), (7), (12), (14b); the open squares represent the DWS data referring to a linearly stratified fluid. The DWS data from experiments intended to treat a two-layer fluid system are also shown (filled squares).

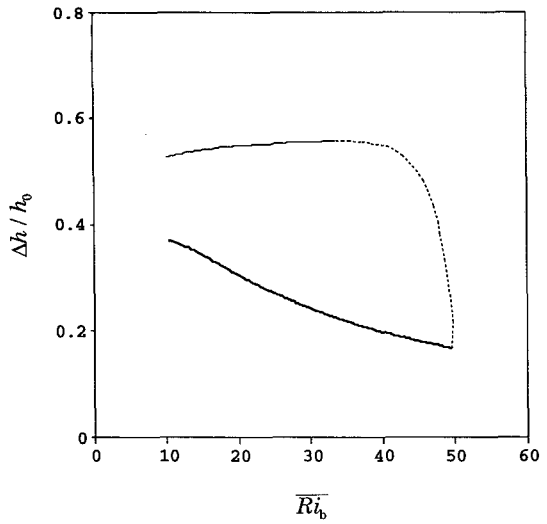

FIG. 14. Convective boundary layer development in a three-layer fluid. The heavy solid curve corresponds to the entrainment in a linearly stratified layer. The dashed curve represents the transition period of the boundary layer development when $\Delta h/h_0$ adjusts to a regime characteristic of a two-layer system. The solid line displays quasi-equilibrium entrainment in a two-layer fluid.

adjustment of the IL to a new regime of entrainment. This is qualitatively illustrated in Fig. 14, showing the results of simulation of entrainment in a three-layer system: the neutral lower layer, linearly stratified layer, and neutral upper layer, with initial values of $\overline{\mathrm{Ri}_b}$ and $\overline{\mathrm{Ri}_N}$ being equal 1 and 25, respectively. The normalized IL depth grows with time during the transition period of the convective boundary layer development, whereas the Richardson number diminishes. It is possible that the DWS measurements refer to this stage.

The model curve in Fig. 14 forms nearly the closed loop. The similar behavior of the interdependencies of the entrainment parameters was observed in the daytime atmospheric boundary layer by Nelson et al. (1989), who called this phenomenon the hysteresis of the entrainment zone.

Another plausible explanation for inverse dependence of $\Delta h/h_0$ on $\overline{\mathrm{Ri}_b}$ in Fig. 12 suggests that the DWS two-layer system experiments were performed on the background of weak stable density stratification in the quiescent layer. The data from Table 1 of DWS indicate that stable lapse rate was always present at the IL top, even in the experiments intended to simulate two-layer fluid. The $\Delta h/h_0$ values from these experiments are plotted against $\overline{\mathrm{Ri}_b}$ in Fig. 13 with due regard to nonzero values of N^2. They conform fairly well with the theoretical curve for a linearly stratified fluid at small $\overline{\mathrm{Ri}_b}$.

It is worth mentioning that the spread of data about the theoretical curve in Fig. 13, obtained with the initial values of Richardson numbers $\overline{\mathrm{Ri}_b} = 1$ and $\overline{\mathrm{Ri}_N} = 4$, is rather large. Equations (6), (7), and (12) indicate that normalized entrainment layer depth is the function of several dimensionless parameters (dimensionless entrainment rate, Richardson numbers, the rate of changes of the IL thickness). Therefore, one can hardly expect empirical data to order well if $\Delta h/h_0$ is presented as a function of the only parameter ($\overline{\mathrm{Ri}_b}$ in Fig. 13). Gryning and Batchvarova (1994) processed the data on $\Delta h/h_0$ in terms of combination $\mathrm{Ri}_E = \bar{E}^{-2}\,\overline{\mathrm{Ri}_b}$, which they called the entrainment Richardson number. This reduced the scatter of empirical points on the graph $\Delta h/h_0$ versus Ri_E as compared to $\Delta h/h_0$ versus $\overline{\mathrm{Ri}_b}$. As follows from the above analysis, $\Delta h/h_0$ may be strongly affected by the nonstationarity of the boundary layer. This effect is not explicitly incorporated by empirical dependence of $\Delta h/h_0$ on $\overline{\mathrm{Ri}_b}$. The data from the DWS experiments processed in terms of $\bar{E}^{-2}\,\overline{\mathrm{Ri}_b}$ are shown in Fig. 15. Taking explicit account of $\bar{E}$ aligns the DWS data with the theoretical predictions of the present model.

6. Conclusions

We have presented the parameterized model for a shear-free convective boundary layer. The model accounts for the buoyancy structure in the entrainment zone. A polynomial approximation for the buoyancy profile within this zone was proposed. The dependence of the profile's integral shape factor on relative stratification was verified against the measurement and LES data.

The entrainment rate equation was derived by considering the turbulent kinetic energy budget and applying the closure hypothesis similar to that proposed by Deardorff (1970a,b). The dimensionless constants were evaluated by integration over the whole turbulized

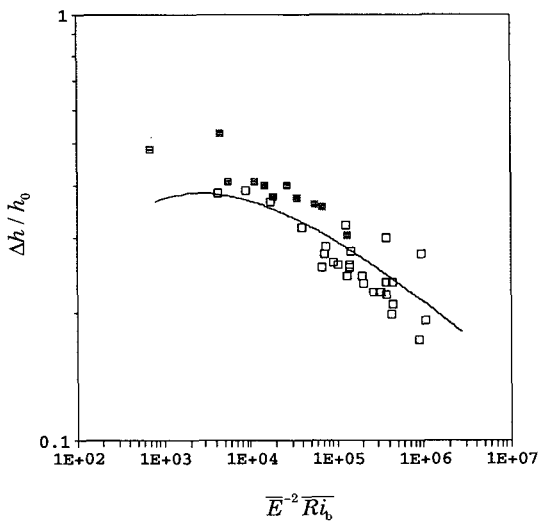

FIG. 15. Normalized entrainment layer depth $\Delta h/h_0$ versus dimensionless combination $\bar{E}^{-2}\overline{\mathrm{Ri}_b}$ in a linearly stratified fluid. The curve is calculated by the present model; the markers are the same as in Fig. 13.

zone of the vertical profiles of turbulent kinetic energy and its dissipation rate, made dimensionless with the length scale $h_0 + \Delta h$ and velocity scale $w_* = [B_s(h_0 + \Delta h)]^{1/3}$. The data from atmospheric, oceanic, and laboratory measurements were used, as well as the results of large-eddy simulations. On average, the estimates using field data exceed the LES and laboratory values. The LES data seem to be most appropriate for the shear-free case.

Two parameterizations for the energy flux at the top of the convective layer due to radiation of internal gravity waves were tested. Equation (14b) appeared to fit the DWS laboratory data a little better than Eq. (14a). However, preference can hardly be given to one of them considering the data scatter.

The model was successfully applied to simulate different regimes of penetrative convection observed in the laboratory. Reasonable explanations for ambiguous behavior of $\Delta h/h_0$ in the DWS experiments with the two-layer fluid were suggested.

The model is able to reproduce the hysteresis-type relationships between the entrainment parameters, resulting from the convective boundary layer development through consecutive transition stages in a multilayer fluid (Fig. 14). Such a behavior of entrainment zone is observed in the atmosphere when the effects of wind shear and large-scale subsidence are weak.

Acknowledgments. The authors gratefully acknowledge useful discussions with Prof. Sergej Zilitinkevich and Dr. Sven-Erik Gryning. Thanks are due to Dr. Paul Mason, Dr. Chin-Hoh Moeng, Prof. Frans Nieuwstadt, and Prof. Ulrich Schumann for providing the authors with large-eddy simulation data and for their valuable comments. During this study the first author was supported by Conseil Régional des Pays de la Loire, France, and, at the last stage of research, by the Alexander von Humboldt Foundation, Germany. The second author acknowledges support from the ICSC World Laboratory.

APPENDIX

Derivation of the Buoyancy Budget and Entrainment Rate Equations

To obtain the ML buoyancy budget equation (6) one should integrate buoyancy transfer equation (5) over z from 0 to h_0, taking into consideration that ML depth h_0 is the time-dependent variable. According to the rules of differentiating integrals with variable limits, the transformation of the left-hand term of (5) leads to

$$\int_0^{h_0} \frac{\partial b}{\partial t}\, dz' = -b|_{h_0} \frac{dh_0}{dt} + \frac{d}{dt}\int_0^{h_0} b dz'. \quad \text{(A1)}$$

While representing the vertical structure of buoyancy we assumed [see Eqs. (3) and (4)] that at $z = h_0$ the buoyancy profile is continuous. In addition, we adopted the constancy of the buoyancy with height within the ML. Then, the expression (A1) can be written as

$$\int_0^{h_0} \frac{\partial b}{\partial t}\, dz' = -b_m \frac{dh_0}{dt} + \frac{d(b_m h_0)}{dt} = h_0 \frac{db_m}{dt}. \quad \text{(A2)}$$

From parameterization (3) and specified conservation of buoyancy profile in the nonturbulent layer it follows that b_m is related to Δb as $b_m = b_0|_{h_0+\Delta h} - \Delta b$. The value of buoyancy at the top of the interfacial layer can be presented in the form $b_0|_{h_0+\Delta h} = b_{0s} + N^2(h_0 + \Delta h)$, where $b_{0s} = \text{const}$ is interpolated value of b_0 at $z = 0$. Thus, the integration of $\partial b/\partial t$ gives

$$\int_0^{h_0} \frac{\partial b}{\partial t}\, dz' = h_0 \frac{d}{dt}[N^2(h_0 + \Delta h) - \Delta b]. \quad \text{(A3)}$$

Integration of $-\partial B/\partial z$ in the right-hand part of (3) yields $B|_{h_0} - B_s$. The first term of this difference equals zero due to the assumption that the level of $B = 0$ defines the top of the ML. Together with (A3) this gives Eq. (6).

The buoyancy budget equation for the whole turbulized zone is derived from similar considerations. Integrating (5) over z from 0 to $h_0 + \Delta h$, we obtain

$$\frac{d}{dt}\int_0^{h_0+\Delta h} b dz' - (b_m + \Delta b)\frac{d(h_0 + \Delta h)}{dt} = B_s. \quad \text{(A4)}$$

Here we set $B|_{h_0+\Delta h} = 0$, employing the fact that turbulent heat flux vanishes at the upper interface of the entrainment layer. The term with the integral in the left-hand part of (A4) can be split in two:

$$\frac{d}{dt}\int_0^{h_0+\Delta h} b dz' = \frac{d(b_m h_0)}{dt} + \frac{d}{dt}\int_{h_0}^{h_0+\Delta h} (b_m + F\Delta b) dz'. \quad \text{(A5)}$$

Presenting b_m in (A5) as $b_m = b_{0s} + N^2(h_0 + \Delta h) - \Delta b$, carrying out sequential integration and differentiation in the second term, and substituting the result in (A4), we come to Eq. (7).

To derive the expression (8) of the buoyancy flux profile in the ML, it is necessary to integrate the buoyancy transfer equation (5) from 0 to $z \leq h_0$, taking into account that b is constant with depth within the ML:

$$\int_0^z \frac{\partial b}{\partial t}\, dz' = z\frac{db_m}{dt} = B_s - B(z), \quad \text{(A6)}$$

and then replace db_m/dt by B_s/h_0, according to (A2) and Eq. (6).

The integration of Eq. (5) from 0 to $z \in [h_0, h_0 + \Delta h]$ gives the representation (9) of the buoyancy flux profile in the entrainment zone.

Expressions (8) and (9) for both parts of the B profile are used in the derivation of the entrainment rate equation (12) by integrating the balance equation (10) for e over z from 0 to $h_0 + \Delta h$. In (12) all terms are normalized by $(B_s h_0)/2$. Taking into account the adopted dimensionless representation of turbulent ki-

netic energy (11), the normalized integral of $\partial e/\partial t$ yields

$$\frac{10}{3}C_e\left(1+\frac{\Delta h}{h_0}\right)^{2/3}(E_h+E_\Delta)+\frac{4}{3}C_e\left(1+\frac{\Delta h}{h_0}\right)^{5/3}De.$$

Integration of $-\partial\Phi/\partial z$ gives $-2\Phi(h_0+\Delta h)/(B_s h_0)$ (we assume that there is no turbulent transport through the underlying surface). Employing the nondimensional form for the dissipation rate profile (11), the integral of ϵ results in $2C_\epsilon(1+\Delta h/h_0)$. Unity in the right-hand part of (12) appears as the result of integrating B profile (8) from 0 to h_0. The other terms in (12) originate from the integration of the buoyancy flux profile (9) over z from h_0 to $h_0+\Delta h$.

REFERENCES

Ball, F. K., 1960: Control of inversion height by surface heating. *Quart. J. Roy. Meteor. Soc.*, **86,** 483–494.

Barenblatt, G. I., 1978: On self-similarity of temperature and salinity distribution in upper thermocline. *Izv. Acad. Sci. USSR, Atmos. Oceanic Phys.*, **14,** 1160–1166.

Batchvarova, E., and S.-E. Gryning, 1991: Applied model for the growth of the daytime mixed layer. *Bound.-Layer Meteor.*, **56,** 261–274.

Betts, A. K., 1973: Non-precipitating cumulus convection and its parameterization. *Quart. J. Roy. Meteor. Soc.*, **99,** 178–196.

——, 1974: Reply to comment on the paper "Non-precipitating cumulus convection and its parameterization." *Quart. J. Roy. Meteor. Soc.*, **100,** 469–471.

Carson, D. J., 1973: The development of dry inversion-capped convectively unstable boundary layer. *Quart. J. Roy. Meteor. Soc.*, **99,** 450–467.

——, and F. B. Smith, 1974: Thermodynamic model for the development of a convectively unstable boundary layer. *Advances in Geophysics,* Vol. 18A, H. E. Landsberg and J. Van Mieghem, Eds., Academic Press, 111–124.

Caughey, S. J., and S. G. Palmer, 1979: Some aspects of turbulence structure through the depth of the convective boundary layer. *Quart. J. Roy. Meteor. Soc.*, **105,** 811–827.

Chorley, L. G., S. J. Caughey, and C. J. Readings, 1975: The development of the atmospheric boundary layer: Three case studies. *Meteor. Mag.*, **104,** 349–360.

Clarke, R. H., A. J. Dyer, R. R. Brook, D. G. Reid, and A. J. Troup, 1971: The Wangara experiment: Boundary layer data. Tech. Paper 19, Div. Meteor. Phys., CSIRO Australia, 363 pp. [NTIS N71-37838.]

Deardorff, J. W., 1970a: Preliminary results from numerical integration of the unstable boundary layer. *J. Atmos. Sci.*, **27,** 1209–1211.

——, 1970b: Convective velocity and temperature scales for the unstable planetary boundary layer and for Raleigh convection. *J. Atmos. Sci.*, **27,** 1211–1213.

——, 1979: Prediction of convective mixed-layer entrainment for realistic capping inversion structure. *J. Atmos. Sci.*, **36,** 424–436.

——, and G. E. Willis, 1985: Further results from a laboratory model of the convective planetary boundary layer. *Bound.-Layer Meteor.*, **32,** 205–236.

——, ——, and D. K. Lilly, 1969: Laboratory investigation of non-steady penetrative convection. *J. Fluid Mech.*, **35,** 7–31.

——, ——, and B. H. Stockton, 1980: Laboratory studies of the entrainment zone of a convectively mixed layer. *J. Fluid Mech.*, **100,** 41–64.

Efimov, S. S., and V. M. Tsarenko, 1980: On a self-similarity of the temperature distribution in the upper thermocline. *Izv. Acad. Sci. USSR, Atmos. Oceanic Phys.*, **16,** 620–627.

Fernando, H. J. S., 1991: Turbulent mixing in stratified fluids. *Annu. Rev. Fluid Mech.*, **23,** 455–493.

Gryning, S.-E., and E. Batchvarova, 1994: Parameterization of the depth of the entrainment zone above the daytime mixed layer. *Quart. J. Roy. Meteor. Soc.*, **120,** 47–58.

Kantha, L. H., 1977: Note on the role of internal waves in thermocline erosion. *Modelling and Predictions of the Upper Layer of the Ocean,* E. B. Kraus, Ed., Pergamon, 173–177.

Kitaigorodskii, S. A., and Y. Z. Miropolsky, 1970: On the theory of open ocean active layer. *Izv. Acad. Sci. USSR, Atmos. Oceanic Phys.*, **6,** 178–188.

Lenschow, D. H., J. C. Wyngaard, and W. T. Pennel, 1980: Mean-field and second-momentum budgets in a baroclinic, convective boundary layer. *J. Atmos. Sci.*, **37,** 1313–1326.

Lilly, D. K., 1968: Models of cloud-topped mixed layers under a strong inversion. *Quart. J. Roy. Meteor. Soc.*, **94,** 292–309.

Linden, P. F., 1975: The deepening of mixed layer in a stratified fluid. *J. Fluid Mech.*, **71,** 385–405.

Mälkki, P., and R. Tamsalu, 1985: Physical features of the Baltic Sea. *Finn. Mar. Res.*, No. 252, 110 pp.

Mason, P. J., 1989: Large-eddy simulation of the convective atmospheric boundary layer. *J. Atmos. Sci.*, **46,** 1492–1516.

Miropolsky, Y. Z., B. N. Filyushkin, and P. P. Chernyshkov, 1970: On the parametric description of temperature profiles in the active ocean layer. *Okeanologiya,* **10,** 1101–1107.

Moeng, C.-H., 1984: A large-eddy simulation for the study of planetary boundary layer turbulence. *J. Atmos. Sci.*, **41,** 2052–2062.

Nelson, E., R. Stull, and E. Eloranta, 1989: A prognostic relationship for entrainment zone thickness. *J. Appl. Meteor.*, **28,** 885–903.

Nieuwstadt, F. T. M., and R. A. Brost, 1986: Decay of convective turbulence. *J. Atmos. Sci.*, **43,** 532–546.

——, P. J. Mason, C.-H. Moeng, and U. Schumann, 1993: Large-eddy simulation of the convective boundary layer: A comparison of four computer codes. *Turbulent Shear Flows 8,* F. Durst et al., Eds., Springer, 343–367.

Reshetova, O. V., and D. V. Chalikov, 1977: On the universal structure of the active layer in the ocean. *Okeanologiya,* **17,** 774–777.

Schmidt, H., and U. Schumann, 1989: Coherent structures of the convective boundary layer derived from large-eddy simulations. *J. Fluid Mech.*, **200,** 511–562.

Shay, T. J., and M. C. Gregg, 1986: Convectively driven turbulent mixing in the upper ocean. *J. Phys. Oceanogr.*, **16,** 1777–1798.

Shapiro, G. I., 1980: Effect of fluctuations in a turbulent entrainment layer on heat and mass transfer in the upper thermocline. *Izv. Acad. Sci. USSR, Atmos. Oceanic Phys.*, **16,** 433–436.

Stull, R. B., 1973: Inversion rise model based on penetrative convection. *J. Atmos. Sci.*, **30,** 1092–1099.

——, 1976: Mixed-layer depth model based on turbulent energetics. *J. Atmos. Sci.*, **33,** 1268–1278.

Tennekes, H., 1973: A model for the dynamics of the inversion above a convective boundary layer. *J. Atmos. Sci.*, **42,** 558–567.

Thorpe, S. A., 1973: Turbulence in stably stratified fluids: A review of laboratory experiments. *Bound.-Layer Meteor.*, **5,** 95–119.

Turner, J. S., 1978: The temperature profile below the surface mixed layer. *Ocean Model,* **11,** 6–8.

Willis, G. E., and J. W. Deardorff, 1974: A laboratory model of the unstable planetary boundary layer. *J. Atmos. Sci.*, **31,** 1297–1307.

Wyatt, L. R., 1978: Mixed layer development in an annular tank. *Ocean Model.*, **17,** 6–8.

Zeman, O., and H. Tennekes, 1977: Parameterization of the turbulent energy budget at the top of the daytime atmospheric boundary layer. *J. Atmos. Sci.*, **34,** 111–123.

Zilitinkevich, S. S., 1975: Comments on "A model for the dynamics of the inversion above a convective boundary layer." *J. Atmos. Sci.*, **32,** 991–992.

——, 1991: *Turbulent Penetrative Convection.* Avebury Technical, Aldershot, 179 pp.

——, and D. V. Mironov, 1992: Theoretical model of the thermocline in a freshwater basin. *J. Phys. Oceanogr.*, **22,** 988–996.

Zubov, N. N., 1945: *Arctic Ices.* Glavsevmorput, Moscow.